PAPER

Scale up of fully eco-friendly zinc–O₂(ads) batteries from the lab scale to the prototype level†

Marcell Árpád Kordován,[a] Tibor Nagy, [ID][a] Gergő Róth,[ab] Dávid Nyul,[ab] Lajos Nagy,[a] Ákos Kuki,[a] Miklós Zsuga[a] and Sándor Kéki [ID] *[a]

Due to their benefits of high specific energy, safety, environmental friendliness and low cost, zinc–air batteries (ZABs) are considered as promising candidates for the next generation of energy storage devices. In this article, we report on the scale-up of our previously developed laboratory cell operating with charcoal cathode and swollen cotton membrane immersed in alkaline electrolyte solution to obtain a multi-cell prototype battery with increased energy density, open-circuit voltage and working discharge current. Furthermore, we designed our battery using adsorbed oxygen (O₂(ads)), allowing the application of a closed system. As a proof of concept, a six-cell battery prototype is developed and built with a capacity of 150 mA h and 148 mW h per cell and an output voltage of 7.5 V. A single cell is tested using galvanostatic, galvanodynamic and electrochemical impedance spectroscopy (EIS) analyses. The invaluable use of distribution of relaxation times (DRT) for rechargeable zinc–air or zinc–O₂(ads) cells is also presented and demonstrated. The EIS Nyquist-plots are evaluated and discussed by means of equivalent circuit models (ECMs) and the DRT method. Further scale-up could aid the development of our zinc–O₂(ads) battery as a low-cost, safe and sustainable technology for deployed energy storage systems (ESS).

1. Introduction

Electrochemical energy storage technologies, particularly batteries, play a key role in addressing the global environmental and societal challenges such as climate change, energy security and reliability as well as environmental sustainability. Improved battery performance is essential for storing and efficiently delivering renewable energy (*e.g.*, from solar and wind sources). In this respect, batteries have to meet a number of requirements, such as high energy and power density, long cycle life, high efficiency and charge rate, *etc.* Moreover, from a global perspective, eco-friendliness is a growing concern. Indicators such as the raw materials used (preferably non-toxic, safe, cheap, and abundant), recyclability, and the overall environmental impact of manufacturing and disposing of the battery should be considered. It is no exaggeration to say that lithium-ion batteries are now an essential part of our everyday lives. However, lithium-ion battery technology is approaching its performance limits, and has several safety and environmental issues.[1,2] Intensive research is therefore underway to

find alternatives that meet all the requirements described above. Due to their advantages of high specific energy, safety, eco-friendliness, and low cost, zinc–air batteries (ZABs) are considered as promising candidates for the next generation of energy storage devices.[3–7] Although primary ZABs are already widely used in various applications,[8] the development of rechargeable, secondary ZABs still faces several challenges that hinder their commercialization.[9] The major issues at the zinc anode are corrosion, passivation, and dendrite formation.[4] If the dendrites grow too large, they can contact the cathode and cause a short circuit. To prevent the formation of dendrite, several strategies are employed, such as application of additives in electrolyte, anode surface modifications and coatings,[10,11] while others focus on more uniform zinc deposition.[12] The corrosion of zinc is an unavoidable process, however, its rate can be decreased by protecting coatings[13] or application of zinc alloys.[14] Passivation can take place if insoluble zinc compounds are accumulated on the surface of zinc anode, this undesirable process can be prevented by electrolyte additives[15] and textured zinc anode surface.[16] On the cathode side, during the charge and discharge process, the oxygen evolution and oxygen reduction reactions (OER and ORR) suffer from sluggish kinetics resulting in high electrode polarization and low current density leading to a large potential gap between OER and ORR. To promote the electrochemical reactions special cathodes are applied such as noble metal containing[17] or carbon based[18] cathodes, the former is expensive, while the latter has limited

[a]Department of Applied Chemistry, Faculty of Science and Technology, University of Debrecen, Egyetem tér 1, H-4032 Debrecen, Hungary. E-mail: keki.sandor@science.unideb.hu; Fax: +36 52 518662

[b]Doctoral School of Chemistry, University of Debrecen, Egyetem tér 1, H-4032 Debrecen, Hungary

† Electronic supplementary information (ESI) available. See DOI: https://doi.org/10.1039/d5ra01434d

activity. Another interesting choice can be the usage of composites and polymer-based materials[19] as cathode. Although these are less expensive, however, their conductivity and/or catalytic activity is limited. The recycling of zinc anodes is well-established due to the commercialization of primary ZABs. However, in terms of environmental sustainability, the entire battery must use cheap, abundant and environmentally friendly materials, especially for the cathode OER and ORR catalysts.

Recently, we reported our novel rechargeable zinc–air cell, which is free of heavy metals and uses biodegradable and commercially available materials.[20–22] It has a swollen cotton fabric cell membrane which, together with the carboxymethyl cellulose sodium salt (CMC-Na) as an additive for the alkaline electrolyte, effectively regulates the ion transport between the anode and the cathode and successfully suppresses the formation of metallic zinc dendrites on the surfaces of the anode. The additive-free pure charcoal acts as an effective catalyst for the OER and ORR of the cathode by adsorbing the oxygen formed "*in situ*". We have assembled a full battery cell and studied the reactions and processes using electrochemical and materials testing methods.

As a continuation, in this work, we take the first step in the scale-up process of our environmentally friendly Zn–air rechargeable battery by increasing the energy density and the working discharge current. As a proof of concept, a six-cell battery prototype is developed and built with an output voltage of 7.5 V. The battery is tested by galvanostatic, galvanodynamic, and electrochemical impedance spectroscopy (EIS) analyses. In addition, to the best of our knowledge, we are the first to apply the distribution of relaxation times (DRT) method to the analysis of rechargeable zinc–air type batteries. Furthermore, we designed our battery using adsorbed oxygen (O_2(ads)), allowing the application of a closed system. It is also showed by electrochemical methods (cycling test, EIS, DRT) that the zinc–O_2(ads) closed cell operates for a long time. In the following, we refer to our designed rechargeable system as zinc–O_2(ads) battery.

2. Experimental section

2.1. Materials

The graphite rod electrode with spectroscopic grade was purchased from Ceramics Praha (Czech Republic, Prague). The nickel plate was purchased from Modul-Elektronika (Hungary, Debrecen). The anode material was a 0.65 mm thick zinc plate (Rheinzink, EN/DIN 988), which was washed in acetone (Molar Chemicals, Hungary, Halásztelek) before use. The potassium hydroxide and zinc oxide were purchased from VWR (Hungary, Debrecen). Activated carbon was obtained from Molar Chemicals Ltd (Halásztelek, Hungary), and the major and minor diameters of the activated carbon particles (supposing ellipse-shaped particles) was calculated to be 13.55 ± 0.08 μm and 7.55 ± 0.04 μm, respectively, using scanning electron microscopy images and ImageJ software. The graphite flakes were obtained from Sigma-Aldrich. The carboxymethyl cellulose Na salt (CMC-Na, Mn: 250 kDa and $f = 1.2$) was obtained from

Merck (Darmstadt, Germany). Fibrology polypropylene (PP) filament was used for 3D printing originated from 3DJake GmbH (Paldau, Austria). Cotton canvas was purchased from a haberdashery shop, and its thickness was measured to be 0.50 mm.

2.2. Construction of Zn–O_2(ads) rechargeable battery cell and battery pack

A 3D printer (Prusa MK3S+; Prague, Czech Republic) was used to produce the battery case, designed by Fusion 360 software (Autodesk, San Francisco, CA, USA). The polypropylene (PP) battery case is resistant to highly alkaline electrolytes and physical impact. The PP used for printing has very good layer adhesion, which is an important parameter due to possible leakage and stability. The 25×50 mm zinc anode plate was cut from zinc foil (thickness 0.65 mm). Using a clamping frame, the cotton separator was sandwiched between the two electrode spaces. The zinc plate was held in place by clamping lugs placed 14.5 mm from the cotton separator. Prior to loading the cathode material, the nickel plate was inserted to act as a collector. The base material of the cathode was a $1:3:10$ mass ratio mixture of activated carbon, graphite flakes, and electrolyte (0.25 M ZnO dissolved in 6 M KOH). The phase of the mixture was paste. The challenges that had to be solved during the battery scale-up procedure were the unstable motion of the cathode paste upon moving the battery, the leakage/evaporation of the lye and the charging of the battery pack. Thus, to avoid the problem of cathode fluctuation, after loading, the cathode material was secured with a clamping plate. The anode space was filled with electrolyte, which was an aqueous 6 M KOH solution containing 0.25 M ZnO and CMC-Na salt (M_w: 250 kg mol^{-1}, functionality: 1.2) at a concentration of 2% (m m^{-1}), to reduce dendrite formation.[21] After electrolyte loading, a safety cap was fitted to both sides of the cell to prevent leakage and evaporation of the electrolyte solution.

Six cells were used to build the battery pack. The cells were placed in a 3D-printed box and connected in series by soldering the appropriate poles. The opposite poles of the two end cells were connected to a standard jack plug attached to the top of the battery cap. A homemade charge controller was designed and constructed. To connect the charge controller, the cell terminals were connected to a printed circuit board (PCB) spike connector, which was also attached to the top of the battery pack.

2.3. Potentiostatic and electrochemical impedance spectroscopy (EIS) measurements

For the battery performance tests, a Biologic SP-150 potentiostat (Seyssinet-Pariset, France) equipped with the EC-LAB software package was used. The charge–discharge tests were performed in the working potential range of 0.7–1.9 V, and charging and discharging currents were varied from 6 to 12 mA cm^{-2}. Galvanodynamic polarisation tests were conducted by increasing the charge and discharge current from 0 to 300 mA and 0 to 400 mA, respectively, at a rate of 2 mA s^{-1}. The full discharge test was carried out at 75 mA discharge current.

Electrochemical impedance spectroscopy measurements were performed at open-circuit voltage (OCV) and at charge/discharge DC currents of 35, 55, and 75 mA. We tested the newly assembled cell and the cell loaded with 200, 400, 600 charge/discharge cycles. The duration of a cycle and the charge/discharge current were 10 min and 75 mA, respectively. To measure the impedance, we used an alternating current with an amplitude of 5 mA in the range of 10 mHz to 100 kHz, 20 points per decade were recorded. Distribution of relaxation time (DRT) calculations were performed using MathWorks Matlab 2023a software. All electrochemical tests were conducted at a constant temperature of 25 °C.

3. Results and discussion

3.1. Development and scale-up

The aim of our laboratory-scale zinc–O_2(ads) battery cell development was to perform material design experiments (*e.g.* electrolyte composition, membrane properties, cathode structure, *etc.*) and to determine the basic cell geometry parameters (*e.g.* electrode surfaces, membrane thickness, *etc.*).[20–22] The conceptual outline of the gaps between our laboratory- and prototype-scale zinc–O_2(ads) battery and the key aspects of the scale-up process are shown in Fig. 1. Application of adsorbed oxygen for the cathode processes made it possible to seal the cell avoiding the leaking of lye and diffusion of harmful air components (such as carbon dioxide) into the cell.

The main goal in scaling up to the prototype level was to reduce the volume/mass of the overall cell, leading to an increase in the proportion of the active materials and energy density. The exploded-drawing of the prototype cell is shown in Fig. 2. At first, the cell geometry was optimized. In the first attempt, a cell with zinc anode dimensions of 50 × 50 × 0.65 mm (width, height, and thickness) and a cathode volume

of 70 cm^3 was tested by galvanostatic charge/discharge cycling at a current density of 6 mA cm^{-2}. As seen in Fig. S1a,† stable operation was obtained over the 60, 2-hour cycles. When the cell was split vertically, the stability of the operation did not change, as shown in Fig. S1b.† In contrast, horizontally halving of the cell (*i.e.*, a quartering compared to the original) the cycle test failed and the charge voltage limit had been already reached in the second cycle and the cycles were subsequently shortened (see Fig. S1c†). Therefore, we returned to the cell with the halved anode (Fig. S1b†) and reduced the volume of the cathode to half as well. As seen in Fig. S1d,† the operation of the cell was stable, even after 50 cycles, the maximum charge voltage of the cycles did not come close to the set limit voltage of 1.9 V. This geometry was chosen for the final version of the cell, as further reductions in size did not result a well-functioning cell taking care of homogeneity of activated carbon slurry (*i.e.* trapped air bubbles). Table 1 summarizes the key parameters of our prototype cell. Comparing the cell parameters obtained with those of liquid[23–31] and solid cells[28–32] found in the literature, it can be concluded that the peak power density of our cell (9 mW cm^{-2}) is lower than the values obtained for other cells (40–300 mW cm^{-2}). However, in these cells special cathodes such as N-doped graphite with nickel and cobalt,[25,26,32] heavy metals (for instance platinum)[23] and manganese-oxide containing cathodes[24] were applied that are too expensive and/or not environmentally friendly for commercial production. Our goal was to design a cheap, heavy metal free and basically green cell. Nevertheless, the energy density calculated by the consumed zinc[32] was found to be more than 400 W h kg^{-1}.

In the next step, six zinc–O_2(ads) cells were connected in series to achieve the standard USB port voltage of 5 V and to increase the power of the prototype battery. A simple home-made battery charge regulator with diodes to protect the cells
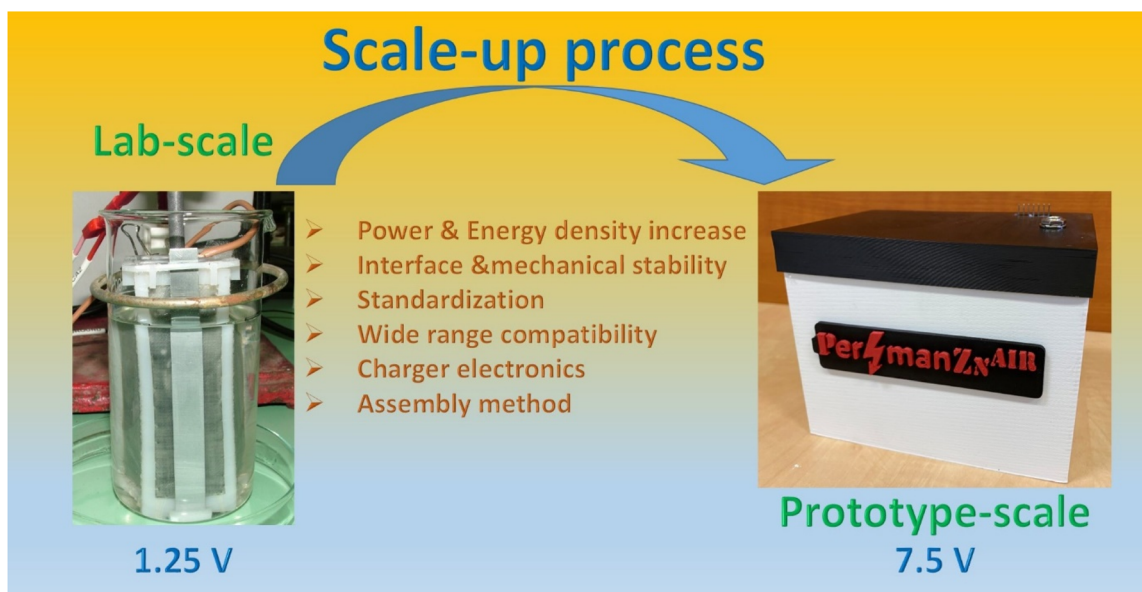

Scale-up process

Lab-scale

➤ Power & Energy density increase
➤ Interface & mechanical stability
➤ Standardization
➤ Wide range compatibility
➤ Charger electronics
➤ Assembly method

1.25 V

Prototype-scale

7.5 V

Fig. 1 Schematic representation of the scale-up process of our zinc–O_2(ads) battery.
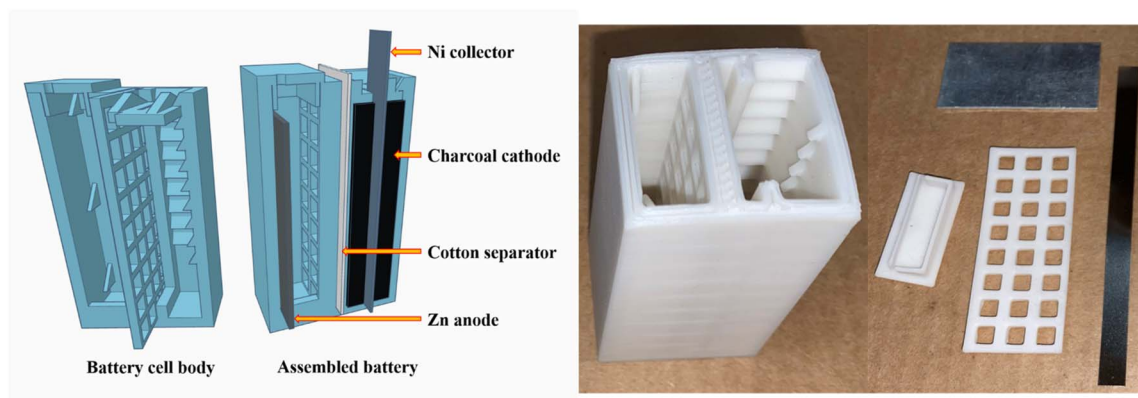
Fig. 2 The exploded-drawing and photographs of the 3D-printed prototype cell.

Table 1 The most important parameters of our zinc–O_2(ads) prototype cell

Name	Value
Anode dimension	$25 \times 25 \times 0.65$ mm
Anode-side volume	18 cm^3
Cathode volume	16 cm^3
Cell OCV	1.25 V
Peak power density	9.0 mW cm^{-2}
Energy efficiency[a]	50.0%
Capacity	150 mA h; 148 mW h

[a] The energy efficiency was determined at 5 mA cm^{-2} charge and 10 mA cm^{-2} discharge current densities.

from being overcharged was used for the charging process (see ESI Fig. S2†).

3.2. Battery-performance evaluation

A variety of experimental testing techniques was used to evaluate the electrochemical performance of our zinc–O_2(ads) battery.[33] A single cell was tested to determine the key parameters, such as the open-circuit voltage (OCV), operating voltage, energy efficiency, specific capacity, energy density, power density, cyclic stability, individual resistance, capacitance and electrode polarization values.

It can be seen in Fig. 3c (cycling test) that the charging potential was below 1.6 V over 500 cycles. It is important to note that the thermodynamic potential of carbon oxidation to carbon-dioxide is 0.207 V *vs.* RHE.[34] Although the thermodynamic potential of the oxidation process is low, it was shown that the reaction rate of the carbon oxidation became significant only above 1.6 V *vs.* RHE.[35,36] Thus, to avoid significant oxidation of carbon, the cell was operated with low potential applied on the cathode. Furthermore, capacity retention was also calculated for cycles (see ESI Fig. S3†), which provides better insight into degradation mechanisms. As it can be seen in Fig. S3,† after 1000 cycles approximately 52% capacity retention was obtained, which is similar to that was found for other cells operating with pristine zinc (59%).[37] The possible

electrochemical reactions of our Zn–O_2(ads) cell are shown in Scheme 1.

3.2.1. Galvanodynamic polarization. The galvanodynamic behavior of our Zn–O_2(ads) battery cell during both charging and discharging is shown in Fig. 3a. The polarization plots representing the battery's operating voltage in response to discharging and charging currents (black lines) start from OCV, *i.e.*, 1.25 V. The polarization curves usually show an initial short, but steep voltage jump (charge) and drop (discharge) ascribed to the overpotential required to overcome the energy barriers of OER and/or ORR, respectively.[33,38] This activation overpotential is also known as charge transfer resistance. As can be seen in Fig. 3a, the initial stages of both the charge and discharge curves are only slightly steeper than the rest of the curve, indicating high activity of the charge transfer reaction on the cathode. The slope of the polarization curves represents the resistance of the cell including the electrolyte, interface, and charge transfer resistances. The initial slight drop in slopes (both charge and discharge), *i.e.*, the decrease in cell resistance, corresponds to the drop in charge transfer resistance with increasing current determined by EIS, as it will be discussed later. As the discharge current is further increased, a linear voltage drop is obtained, indicating that the cell performance is dominated by the ohmic losses. This linear stage is the desirable operating region for the zinc–air battery.[33] Usually, a sharp voltage drop terminates this linear ohmic regime indicating the insufficient mass transfer of reactants (*i.e.*, oxygen) to the cathode, referred to as mass-transfer polarization or diffusion overpotential. In our zinc–O_2(ads) cell, even at higher current densities, diffusion on the electrodes is not a limiting factor, but rather the performance is reduced by the voltage drop due to ohmic resistance. It should be mentioned that the cell resistances calculated as the derivative of the polarization curves are in the range of 2–6 ohms and these values are in good agreement with those determined by EIS.

The dependence of the power density on the current density (blue line) can be determined from the discharge curve. As seen in Fig. 3a, the maximum power density of a single cell is 9.0 mW cm^{-2}. Based on the galvanodynamic polarization experiments, the energy efficiency of the cell at a given current density can
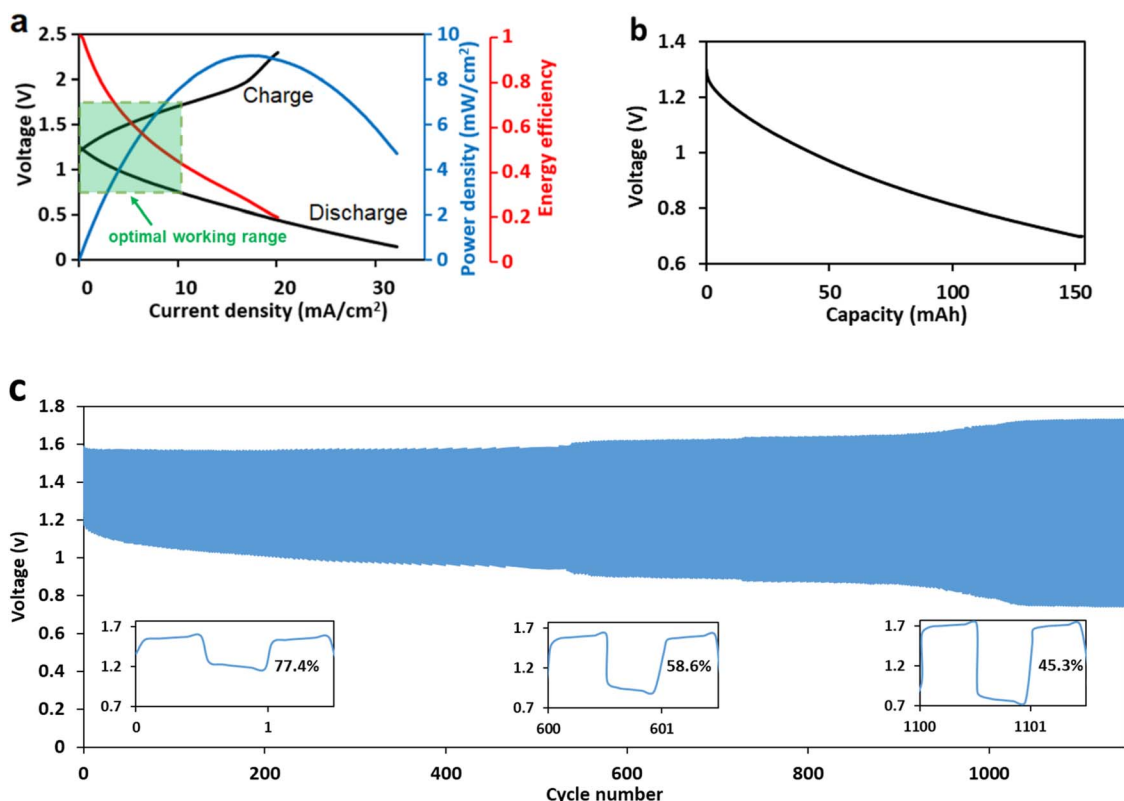
Fig. 3 Performance of a single zinc–O_2(ads) battery cell. (a) Charge and discharge polarization (black), power density (blue), and energy efficiency (red) curves. Optimal working range is shown by green area. (b) Galvanostatic full discharge curve at a current density of 12 mA cm^{-2}. (c) Galvanostatic charge/discharge battery cycling tests applying 12 mA cm^{-2} and 10 min as the current density and duration of a cycle, respectively. The insets compare the round-trip efficiencies at the beginning, middle and end of the cycle test.

also be determined as the ratio of the discharge and charge voltage (red line). Of course, the practical energy efficiency of the cell may change if the charge and discharge current densities are not identical (see Table 1). Remarkably, Wang *et al.* obtained the same discharge and power density curves for their Zn–air battery with an oxygenated carbon cathode.[39]
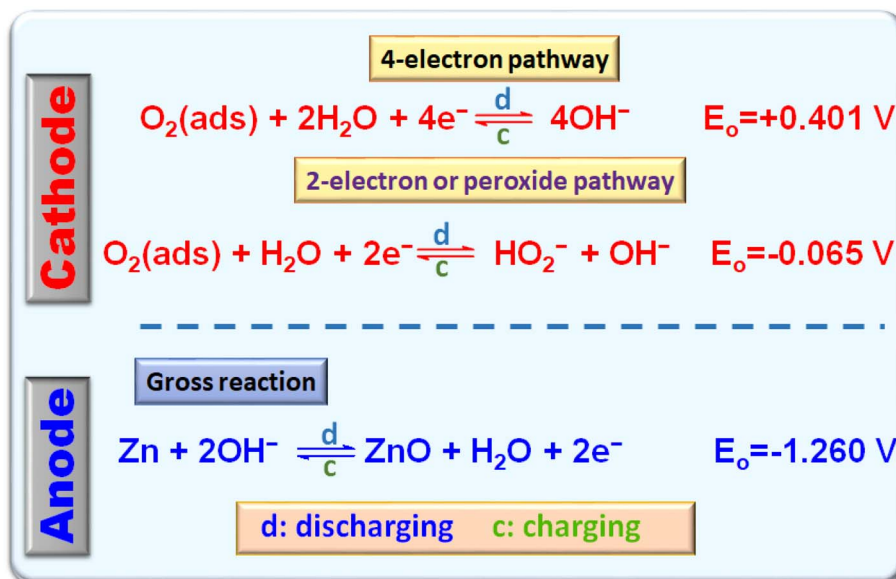
Scheme 1 Typical anode and cathode reactions in the rechargeable Zn–O_2(ads) battery.

3.2.2. Galvanostatic full discharge. The energy storage capacity of our Zn–O$_2$(ads) battery cell was determined by galvanostatic full discharge at a fixed current of 75 mA, corresponding to an anode current density of 12 mA cm^{-2}, until the preset cut-off voltage of 0.7 V was reached. The cutoff voltage was set so that a battery pack with 6 cells in series would deliver the 5 V USB standard voltage with a lower tolerance of 4.2 V. As seen in Fig. 3b, the cell has a capacity of about 150 mA h at the discharge current density of 12 mA cm^{-2}. Integrating the actual power over the discharge time yields an energy of 148 mW h for a single cell.

3.2.3. Galvanostatic cycling. Cycling durability was investigated by galvanostatic charge and discharge tests at 12 mA cm^{-2} (10 min per cycle) over a period of 190 h (1150 cycles, see Fig. 3c). Our Zn–O$_2$(ads) battery shows an extremely narrow charge/discharge potential gap of 0.42 V for the first cycle, suggesting excellent OER and ORR performance of the cathode. After 600 cycles, the gap was still only 0.71 V, while towards the end of the cycling test (after 1100 cycles) the gap reached 0.98 V. The decaying rate of the battery was calculated to be only 0.5 mV per cycle, implying a remarkable long-term cyclability. Calculating the ratio between the charging and discharging potentials, namely the round-trip efficiencies, 77.4%, 58.6%, and 45.3% were obtained for the 1st, 600th, and 1100th charge/discharge cycle.

3.2.4. Electrochemical impedance spectroscopy. To gain further insight into the mechanisms of the zinc–O$_2$(ads) battery cell, electrochemical impedance spectroscopy (EIS) measurements were also carried out. EIS can reveal not only the impedance components of the battery but also the dynamic processes taking place in it. Furthermore, as a comparative technique, EIS can provide additional information on the degradation of different battery elements. For the interpretation and quantification of the EIS spectra, two main approaches were used: fitting an equivalent circuit model (ECM) on the impedance data and/or using the distribution of relaxation times (DRT) method that converts the impedance spectra from the frequency domain to the relaxation time domain. However, in order to perform a meaningful analysis of the impedance spectra and to obtain reliable results, the validity of the EIS data must be checked. The Kramers–Kronig validation test (KK-test) is a powerful tool for filtering out the points that do not meet the linearity, causality, and stability criteria.[40–42] We used the "KK test for Windows" software to check the compliance of the measured data with the Kramers–Kronig transformation rules.[43,44] As a representative example, Fig. S4 and S5† in the ESI show the KK-test plots of the EIS data of a battery cell recorded after 200 cycles, at open-circuit voltage (OCV). As seen in Fig. S4,† the measured and KK-transformed impedance data don not match at low frequencies, *i.e.*, below about 1 Hz. The residuals of the KK-test show the same trend, as seen in the ESI Fig. S5.† When the impedance measurements were performed during a DC charge and discharge, the KK-test failed even at higher frequencies (from about 6 Hz), most probably due to the fact that the system became time-varying with the constant DC components. Consequently, the impedance points below 1 Hz

and 6 Hz were filtered out from the spectra recorded at OCV and under charge/discharge, respectively. These filtered data files were then used to evaluate the EIS measurements by means of the ECM fitting and DRT methods. For comparison, EIS was carried out at different charge/discharge DC currents and after different cycle loads. Fig. 4 shows some examples for the Nyquist- and DRT-plots and multi-curve diagrams for comparison, where the DC current or the number of charge/discharge cycles (done prior to the measurement) was varied. Additional EIS plots are presented in the ESI as Fig. S6 and S7.†

As can be seen in Fig. 4, S6 and S7,† the Nyquist-plots consist of a semicircle, which is typical for electrochemical systems controlled by kinetic processes, and a Randles circuit is commonly used as a reliable equivalent circuit in their study and modelling.[45,46] For the EIS performed at a DC charge/discharge current a simplified Randles circle was used for ECM modelling, since the low frequency points were filtered out. In this model, Fig. 4a inset, R_s, R_{ct}, Q_{dl} represent the ohmic resistance of the cell, the charge transfer resistance describing the rates of electrochemical reactions and the double layer capacitance associated with the electrode/electrolyte interface. As seen in Fig. 4, the semicircles are depressed, suggesting that they are formed by more than one process and/or some physical property of the system is not homogeneous. Therefore, the double layer capacitance is modelled with a constant phase element (CPE) instead of an ideal capacitance. Although a full cell, *i.e.*, both the anode and the cathode processes are measured and modelled, this simple model with a single RQ circuit is justified because air electrode impedance is usually much larger than that of the zinc electrode and electrolyte due to the more difficult gas diffusion and chemical reaction process above the air electrode.[47–49] This assumption was verified by the EIS measurement of a zinc–zinc cell, and proved to be valid in our case, as can be seen from the Bode-plot comparing the impedances of a zinc–zinc cell with that of a zinc–O$_2$(ads) cell (see ESI Fig. S8†). According to the Bode-plot shown at low frequencies (Fig. S8†), which can be used to derive some important cell processes such as gas diffusion, a significantly higher impedance was obtained for the Zn–air cell than for the Zn–Zn cell indicating a higher impedance of the cathode. In the spectra recorded at OCV, there are more valid low frequency points that allows the extension of ECM by an additional CPE element (Q_W) associated with the diffusion processes on the electrodes (see Fig. 4c inset). We would like to point out that a diffusion process is usually modelled by the ECM element Warburg impedance, which is a CPE with a phase of 45°, but we have chosen a general CPE that can better model the more complex processes. The values of the fitted ECM parameters are reported in the ESI as Table S1.† The ohmic resistance (R_s) – the real axis intercept of the Nyquist-plots at high frequencies in Fig. 4 – of our zinc–O$_2$(ads) battery cell is remarkably low and invariant, ranging from 0.61 to 0.65 V at all the DC and cyclic loads. Comparing the Nyquist curves recorded at charging and discharging with the same parameters (DC, cyclic load), one would conclude that there is no significant difference between the charge/discharge processes (see Fig. 4a). However, the paired t-test for the corresponding charge transfer
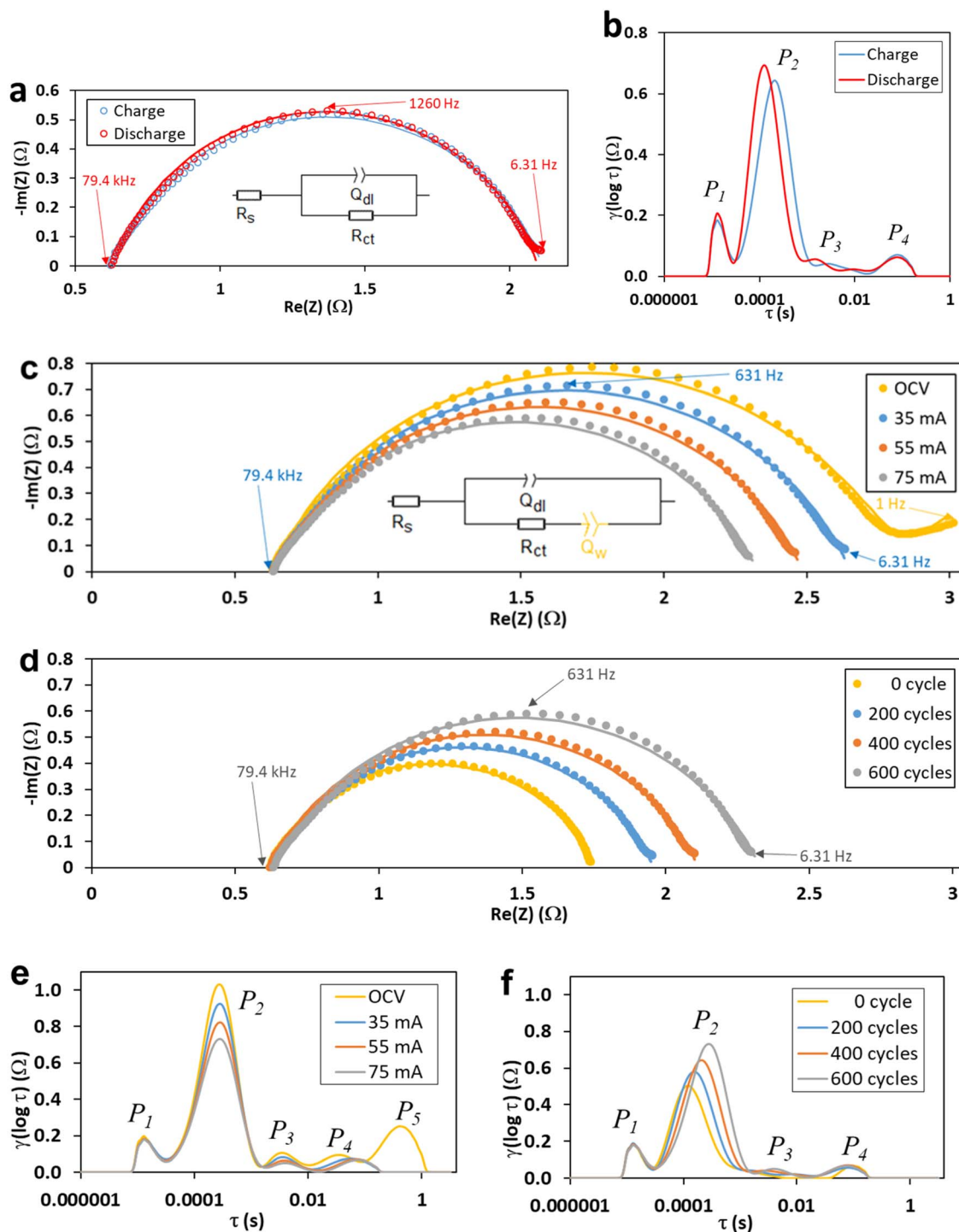
Fig. 4 Nyquist-plots obtained by EIS of a single zinc−O$_2$(ads) battery cell (a) recorded after 400 cycles at a DC current of 75 mA during charging and discharging. The solid lines represent the fitted impedance data using the ECM shown in the inset; (b) DRT plots corresponding to (a); (c) Nyquist-plots at various charge DC currents and at OCV after 600 cycles. The solid lines represent the fitted impedance data using the ECM shown in the inset; (d) Nyquist-plots after different cycling loads at 75 mA charge DC current; (e) DRT plots corresponding to (c); (f) DRT plots corresponding to (d).

resistance values (shown in Table S1†) shows that R_{ct} is significantly greater when the cell is under charge load ($p < 0.0001$). Performing the paired t-test for the time constant values calculated by eqn (1) the result is the same, the τ values under charging are significantly greater ($p = 0.0025$).

$$\tau = (R_{ct}Q_{dl})^{1/n} \tag{1}$$

Fig. 5 The prototype battery, with six zinc−O$_2$(ads) cells connected in series powering the text 'DE TTK' (the acronym for our university and faculty in Hungarian), formed by 51 LEDs.

The lower R_{ct} and τ values indicate the more efficient charge transfer kinetics of the ORR (discharging) compared to the OER (charging).

The comparison and evaluation of the corresponding charge/discharge Nyquist-plots (Fig. 4a) is a good example of how the DRT method can provide additional information compared to the ECM method. (i) First of all, DRT does not require the assumption of a physical or electrical model prior to analyzing of the EIS data. (ii) As mentioned, the semicircle of the Nyquist-plot is depressed, suggesting that it is formed by more than one process, therefore, a single RC time constant is not sufficient for characterization, but we must take into account the distribution of the relaxation times. As can be seen in Fig. 4b, DRT reveals 4 peaks corresponding to 4 processes, or even more if they are overlapped. Here, we should note that a drawback of the DRT method is, that the information obtained, i.e., the number of peaks in the DRT spectrum depends strongly on the choice of the regularization parameter λ used in the DRT calculation. As the regularization parameter decreases, the DRT represents the measurement data more accurately, resulting in sharper peaks. However, a very low λ leads to artificial peaks caused by measuring uncertainty.[50] Therefore, we determined the regularization parameter by lowering λ until the sum of square residuals of the DRT regression stops decreasing (see the ESI, Fig. S9†).[51] The time constants of the $R_{ct}Q_{dl}$ circuit of the ECM shown in Fig. 4a and calculated by eqn (1) are $\tau_c = 0.00018$ s and $\tau_d = 0.00013$ s for the charge and discharge process, respectively, corresponding to the relaxation time of the main peak of the DRT $\tau_{c,2} = 0.00022$ s and $\tau_{d,2} = 0.00013$ (Fig. 4b), of the dominant charge transfer process. Two additional smaller peaks in the mid-frequency range, P$_3$ and P$_4$, are assumed to belong to a less dominant charge transfer processes. The high frequency peak P$_1$ can be attributed to the

ion transport taking place at the membrane and electrode interfaces.[52,53] The DRT analysis of the EIS spectra recorded at OCV containing valid low frequency points reveals another low frequency peak (see Fig. 4e as P$_5$) corresponding to the diffusion processes on the electrodes. (iii) Comparing Fig. 4a and b, it is obvious that the DRT analysis, unlike the ECM method, clearly indicates the differences in dynamic behavior between charge and discharge. The shift of the main DRT peak means a shorter relaxation time of the dominant charge transfer process under discharge, indicating a more efficient kinetics. Furthermore, the area under this peak calculated from eqn (2), represents the real part of the impedance corresponding to the electrochemical process, i.e., the charge transfer resistance.

$$R = \int \gamma(\ln \tau) d\ln \tau \qquad (2)$$

Approximate integration of the dominant peaks in Fig. 4b gives 1.23 Ω and 1.19 Ω for the charge and discharge, respectively, which agrees well with the corresponding charge transfer resistances 1.49 Ω and 1.47 Ω obtained by ECM. The slightly lower resistance when discharging also indicates the higher charge transfer efficiency compared to charging.

Comparing the Nyquist-plots recorded at different DC charge/discharge currents, a clear trend can be seen in Fig. 4c. Namely as the DC load increases, the diagonal of the semicircles representing R_{ct} decreases (see also in Table S1 and Fig S7†). Similar trend has been reported elsewhere for the dependence of the charge transfer resistance on the applied DC current density.[54,55] This supports our assumption that charge transfer can be assigned to the arc of the Nyquist-plots as the main process. The same conclusion can also be drawn from the DRT plots (see Fig. 4e), the area under P$_2$, i.e., the charge transfer resistance, decreases as the DC current increases. However, P$_2$ shows no change in τ, indicating a reverse trend in the double layer capacitance, i.e., an increase as the applied DC current increases, as does the charge transfer resistance (see eqn (1)). As seen in Fig. 4d, f and Table S1,† the performance of the cell decreases with cycling, as indicated by the increase in both the charge transfer resistance and the time constant of P$_2$. It should be noted, however, that the resistance values between 1.7 and 2.2 ohms obtained after 600 cycles are still considered to be quite low. Moreover, as seen in Fig. 4d, the value of the ohmic resistance (R_s) still remained low (<0.65 Ω) during the cycling load, suggesting high cycling stability of the cell. For better visualization, changing of ohmic resistance (R_s), charge transfer resistance (R_{ct}) and the time constant (tau, τ) of P$_2$ was plotted against the cycles (see Fig. S10 of the ESI†).

3.3. Proof of concept application

As a proof of concept, a prototype battery was designed and built using six zinc−O$_2$(ads) cells connected in series to produce an output voltage of 7.5 V. This configuration ensures that the battery voltage does not drop below 5 V under load and a standard USB-A 2.0 port can be used to connect to the system. A 7-pin PCB (printed circuit board) connector with a 2.54 mm pitch is located on the top of the battery pack. This allows the charging electronics to be connected. In addition, there is

a 5.5 mm DC jack socket for supplying the power. To demonstrate the feasibility of our battery in a real environment, the text 'DETTK' (the acronym for our university and faculty in Hungarian), formed by 51 LEDs, was powered as shown in Fig. 5. The overall mass of the prototype is 0.775 kg and the specific energy is 1.15 W h kg^{-1} while the energy density is 0.96 W h L^{-1}. In our prototype there may be no air inlet, the oxygen stored on the cathode is used. In our concept the high energy may be challenging to achieve because the O_2 is not from the air. However, the oxygen is readily available and problems arising from ambient pollutants can be avoided.

4. Conclusions

As a result of the scale-up, a multi-cell prototype battery consisting of six rechargeable Zn–O_2(ads) alkaline cells was created. The battery is free of heavy metals and utilizes biodegradable and commercially available materials. A single cell was tested using galvanostatic, galvanodynamic and electrochemical impedance spectroscopy (EIS) methods and the main parameters were determined. Our zinc–O_2(ads) prototype battery has an open-circuit voltage of 7.5 V, a peak power density of 9 mW cm^{-2}, capacity of 150 mA h and 888 mW h (specific capacity: 1.15 W h kg^{-1}, 30 W h kg$_{zinc}^{-1}$). Increasing the specific capacity through battery design may be the next step in the research progress. The electrochemical measurements have revealed that our battery has a remarkable long-term cyclability (more than 1000 cycles over a period of 190 hours), narrow charge/discharge potential gap ranging from 0.61 to 0.65 V per cell and a strikingly low ohmic resistance, depending on the DC and cyclic loads. Furthermore, the low charge transfer resistance values, even after long cycling, indicate efficient charge transfer kinetics for both ORR and OER processes, which are critical for the zinc–air or zinc–O_2(ads) cells. This proves that the additive-free pure charcoal applied to the cathode side acts as an effective catalyst by adsorbing the oxygen formed "*in situ*". Furthermore, we have successfully applied the distribution of relaxation times (DRT) method to the electrochemical characterization of full zinc–air rechargeable battery cells. We have found that when DRT and equivalent circuit models (ECMs) are used together, they complement each other and are able to provide reliable conclusions. We believe that by continuing the scale-up process, our zinc–O_2(ads) battery can serve as a low-cost, safe and sustainable technology for deployed energy storage systems (ESS).

Data availability

The data supporting this article have been included as part of the ESI.†

Author contributrions

Conceptualization: M. Á. K., T. N., Á. K., M. Zs., S. K., data curation: M. Á. K., G. R., D. Ny., L. N., Á. K., formal analysis: M. Á. K., Á. K., investigation: M. Á. K., G. R., D. Ny., L. N., Á. K., supervision: T. N., Á. K., M. Zs., S. K., visualization: M. Á. K., L. N., Á. K., writing – M. Á. K., T. N., Á. K., original draft, writing – review editing: M. Zs., S. K.

Conflicts of interest

The authors declare no competing interest.

Acknowledgements

References

1 R. Van Noorden, The rechargeable revolution: A better battery, *Nature*, 2014, **507**(7490), 26–28, DOI: **10.1038/507026a**.

2 M. Armand and J. M. Tarascon, Building better batteries, *Nature*, 2008, **451**(7179), 652–657, DOI: **10.1038/451652a**.

3 Y. Li and J. Lu, Metal–Air Batteries: Will They Be the Future Electrochemical Energy Storage Device of Choice?, *ACS Energy Lett.*, 2017, **2**(6), 1370–1377, DOI: **10.1021/acsenergylett.7b00119**.

4 N. Borchers, S. Clark, B. Horstmann, K. Jayasayee, M. Juel and P. Stevens, Innovative zinc-based batteries, *J. Power Sources*, 2021, **484**, 229309, DOI: **10.1016/j.jpowsour.2020.229309**.

5 J. Chang, G. Wang and Y. Yang, Recent Advances in Electrode Design for Rechargeable Zinc–Air Batteries, *Small Sci.*, 2021, **1**(10), 2100044, DOI: **10.1002/smsc.202100044**.

6 Q. Liu, Z. Pan, E. Wang, L. An and G. Sun, Aqueous metal-air batteries: Fundamentals and applications, *Energy Storage Mater.*, 2020, **27**, 478–505, DOI: **10.1016/j.ensm.2019.12.011**.

7 T. Li, M. Huang, X. Bai and Y.-X. Wang, Metal–air batteries: A review on current status and future applications, *Prog. Nat. Sci.: Mater. Int.*, 2023, **33**(2), 151–171, DOI: **10.1016/j.pnsc.2023.05.007**.

8 G. G. Yadav, X. Wei and M. Meeus, Chapter 3 - Primary zinc-air batteries, in *Electrochemical Power Sources: Fundamentals, Systems, and Applications*, ed. H. Arai, J. Garche and L. Colmenares, Elsevier, 2021, pp. 23–45, DOI: **10.1016/B978-0-444-64333-9.00003-5**.

9 A. R. Mainar, E. Iruin, I. Urdampilleta, H.-J. Grande and J. A. Blázquez, Effect of cell design on the durability of secondary zinc-air batteries, *Appl. Energy*, 2024, **353**, 122049, DOI: **10.1016/j.apenergy.2023.122049**.

10 X. Huyan, Z. Yi, Z. Sang, S. Tan, J. Liu, R. Chen, W. Si, J. Liang and F. Hou, Polyethylene glycol coating on zinc powder surface: Applications in dendrite-free zinc anodes with enhanced utilization rate, *Appl. Surf. Sci.*, 2023, **614**, 156209, DOI: **10.1016/j.apsusc.2022.15620**.

11 K. Wang, Y. Zuo, P. Pei, X. Liu, M. Wei, Y. Xiao, J. Xiong and P. Zhang, Zn–Ni reaction in the alkaline zinc-air battery using a nickel-supported air electrode, *Mater. Today*

Energy, 2021, **21**, 100823, DOI: **10.1016/ J.MTENER.2021.100823**.

12 Y. Zuo, K. Wang, P. Pei, M. Wei, X. Liu, Y. Xiao and P. Zhan, Zinc dendrite growth and inhibition strategies, Zinc dendrite growth and inhibition strategies, *Mater. Today Energy*, 2021, **20**, 100692, DOI: **10.1016/ J.MTENER.2021.100692**.

13 A. Naveed, A. Ali, T. Rasheed, X. Wang, P. Ye, X. Li, Y. Zhou, S. Mingru and Y. Liu, Revisiting recent and traditional strategies for surface protection of Zn metal anode, *J. Power Sources*, 2022, **525**, 231122, DOI: **10.1016/ J.JPOWSOUR.2022.231122**.

14 X. Yuan, C. He, J. Wang, X. You, Y. Chen, Q. Gou, N. Yang, G. Xie and Y. Hou, Inhibition of zinc dendrite growth in zinc-air batteries by alloying the anode with Ce and Yb, *J. Alloys Compd.*, 2024, **970**(5), 172523, DOI: **10.1016/ j.jallcom.2023.172523**.

15 H. Pourzolfaghar, S. Hosseini, F. M. Zuki, M. Alinejad and Y. Y. Li, Recent advancements to mitigate zinc oxide formation in zinc-air batteries: A technical review, *Mater. Today Commun.*, 2021, **29**, 102954, DOI: **10.1016/ J.MTCOMM.2021.102954**.

16 J. Yi, P. Liang, X. Liu, K. Wu, Y. Liu, Y. Wang, Y. Xia and J. Zhang, Challenges, mitigation strategies and perspectives in development of zinc-electrode materials and fabrication for rechargeable zinc–air batteries, *Energy Environ. Sci.*, 2018, **11**, 3075–3095, DOI: **10.1039/ C8EE01991F**.

17 M. Gao, C. Li, R. Wang, S. Xiao, Z. Guo and Y. Wang, Noble metal catalysts for metal-air batteries: From nano-level to atom-level, *Next Mater.*, 2024, **2**, 100126, DOI: **10.1016/ J.NXMATE.2024.100126**.

18 Y. Liu, J. Lu, S. Xu, W. Zhang and D. Gao, Carbon-based composites for rechargeable zinc-air batteries: A mini review, *Front. Chem. Sec. Electrochemistry*, 2022, **10**, 1074984, DOI: **10.3389/FCHEM.2022.1074984**.

19 L. Yu, Q. Yi, X. Yang and X. Zhou, One-Step Construction of Ni/Co-Doped C–N Nanotube Composites as Excellent Cathode Catalysts for Neutral Zinc–Air Battery, *Nano*, 2019, **14**(03), 1950028, DOI: **10.1142/S1793292019500280**.

20 T. Nagy, L. Nagy, Z. Erdélyi, E. Baradács, G. Deák, M. Zsuga and S. Kéki, Environmentally friendly Zn-air rechargeable battery with heavy metal free charcoal based air cathode, *Electrochim. Acta*, 2021, **368**, 137592, DOI: **10.1016/ j.electacta.2020.137592**.

21 T. Nagy, L. Nagy, Z. Erdélyi, E. Baradács, G. Deák, M. Zsuga and S. Kéki, Environmentally friendly high performance Zn-air rechargeable battery using cellulose derivatives: A 3D-printed prototype, *J. Energy Storage*, 2022, **49**, 104173, DOI: **10.1016/j.est.2022.104173**.

22 T. Nagy, L. Nagy, Z. Erdélyi, E. Baradács, G. Deák, M. Zsuga and S. Kéki, "In Situ" Formation of Zn Anode from Bimetallic Cu-Zn Alloy (Brass) for Dendrite-Free Operation of Zn-Air Rechargeable Battery, *Batteries*, 2022, **8**(11), 212, DOI: **10.3390/batteries8110212**.

23 S. Zhao, T. Liu, Y. Zuo, M. Wei, J. Wang, Z. Shao, D. Y. C. Leung, T. Zhao and M. Ni, High-Power-Density and High-Energy-Efficiency Zinc-Air Flow Battery System for Long-Duration Energy Storage, *Chem. Eng. J.*, 2023, **470**, 144091, DOI: **10.1016/j.cej.2023.144091**.

24 N. Radenahmad, R. Khezri, A. A. Mohamad, M. T. Nguyen, T. Yonezawa, A. Somwangthanaroj and S. Kheawhom, A durable rechargeable zinc-air battery via self-supported MnOx-S air electrode, *J. Alloys Compd.*, 2021, **883**(25), 160935, DOI: **10.1016/j.jallcom.2021.160935**.

25 M. Gopalakrishnan, W. Kao-ian, M. Rittiruam, S. Praserthdam, P. Praserthdam, W. Limphirat, M. T. Nguyen, T. Yonezawa and S. Kheawhom, 3D Hierarchical MOF-Derived Defect-Rich NiFe Spinel Ferrite as a Highly Efficient Electrocatalyst for Oxygen Redox Reactions in Zinc–Air Batteries, *ACS Appl. Mater. Interfaces*, 2024, **16**(9), 11537–11551, DOI: **10.1021/acsami.3c17789**.

26 H. Liu, J. Huang, K. Feng, R. Xiong, S. Ma, R. Wang, Q. Fu, M. Rafique, Z. Liu, J. Han, D. Hua, J. Li, J. Zhong, X. Wang, Z. Zhao, T. Yao, S. Jiang, P. Xu, Z. Zhang and B. Song, Reconstructing the Coordination Environment of Fe/Co Dual-atom Sites towards Efficient Oxygen Electrocatalysis for Zn–Air Batteries, *Angew. Chem., Int. Ed.*, 2025, **64**, e202419595, DOI: **10.1002/anie.202419595**.

27 J. Wang, X. Q. Fang, J. N. Liu, J. W. Song, M. Zhao, B. Q. Li and J. Q. Huang, Enabling High-Rate and Long-Cycling Zinc–Air Batteries with a $\Delta E = 0.56$ V Bifunctional Oxygen Electrocatalyst, *Adv. Funct. Mater.*, 2025, **35**, 2413562, DOI: **10.1002/adfm.202413562**.

28 S. Surendran, Y. Lim, S. Lee, S. C. Jesudass, G. Janani, H. Choi, G. Kwon, K. Jin and U. Sim, Understanding the Engineering Tactics to Achieve the Stabilized Anode in Next-Generation Zn-Air Batteries, *Exploration*, 2025, 20240054, DOI: **10.1002/EXP.20240054**.

29 P. Zhang, M. Wei, K. Wang, H. Wang, Y. Zuo and M. Zhang, Performance optimization of zinc-air batteries via nanomaterials, *Energy Storage Mater.*, 2025, **75**, 104109, DOI: **10.1016/j.ensm.2025.104109**.

30 S. Ponnada, M. S. Kiai, R. Krishnapriya, R. Singhal and R. K. Sharma, Lithium-Free Batteries: Needs and Challenges, *Energy Fuels*, 2022, **36**(12), 6013–6026, DOI: **10.1021/acs.energyfuels.2c00569**.

31 S. Ponnada and S. Naskar, Advanced Two-Dimensional Material-Based Heterostructures, in *Sustainable Energy Storage Devices*, CRC Press, 1st edn, 2024, DOI: **10.1201/ 9781003404729**.

32 Q. Wang, Q. Feng, Y. Lei, S. Tang, L. Xu, Y. Xiong, G. Fang, Y. Wang, P. Yang, J. Liu, W. Liu and X. Xiong, Quasi-solid-state Zn-air batteries with an atomically dispersed cobalt electrocatalyst and organohydrogel electrolyte, *Nat. Commun.*, 2022, **13**, 3689, DOI: **10.1038/s41467-022-31383-4**.

33 J. Fu, Z. P. Cano, M. G. Park, A. Yu, M. Fowler and Z. Chen, Electrically Rechargeable Zinc–Air Batteries: Progress, Challenges, and Perspectives, *Adv. Mater.*, 2017, **29**(7), 1604685, DOI: **10.1002/adma.201604685**.

34 S. Maass, F. Finsterwalder, G. Frank, R. Hartmann and C. Merten, Carbon support oxidation in PEM fuel cell cathodes, *J. Power Sources*, 2008, **176**(2), 444–451, DOI: **10.1016/j.jpowsour.2007.08.053**.

35 S. Möller, S. Barwe, J. Masa, D. Wintrich, S. Seisel, H. Baltruschat and W. Schuhmann, Online Monitoring of Electrochemical Carbon Corrosion in Alkaline Electrolytes by Differential Electrochemical Mass Spectrometry, *Angew. Chem., Int. Ed.*, 2020, **59**(4), 1585–1589, DOI: **10.1002/anie.201909475**.

36 A. Kundu, S. Mallick, S. Ghora and C. R. Raj, Advanced Oxygen Electrocatalyst for Air-Breathing Electrode in Zn-Air Batteries, *ACS Appl. Mater. Interfaces*, 2021, **13**(34), 40172–40199, DOI: **10.1021/acsami.1c08462**.

37 G. Nazir, A. Rehman, J. H. Lee, C. H. Kim, J. Gautam, K. Heo, S. Hussain, M. Ikram, A. A. AlObaid, S. Y. Lee and S. J. Park, A Review of Rechargeable Zinc–Air Batteries: Recent Progress and Future Perspectives, *Nano-Micro Lett.*, 2024, **16**, 138, DOI: **10.1007/s40820-024-01328-1**.

38 X. Chen, Z. Zhou, H. E. Karahan, Q. Shao, L. Wei and Y. Chen, Recent Advances in Materials and Design of Electrochemically Rechargeable Zinc–Air Batteries, *Small*, 2018, **14**(44), 1801929, DOI: **10.1002/smll.201801929**.

39 W. Wang, Y. Hu, Y. Liu, Z. Zheng and S. Chen, Self-Powered and Highly Efficient Production of H2O2 through a Zn–Air Battery with Oxygenated Carbon Electrocatalyst, *ACS Appl. Mater. Interfaces*, 2018, **10**(38), 31855–31859, DOI: **10.1021/acsami.8b11703**.

40 R. d. L. Kronig, On the Theory of Dispersion of X-Rays, *J. Opt. Soc. Am.*, 1926, **12**(6), 547–557, DOI: **10.1364/JOSA.12.000547**.

41 H. A. Kramers, Zur Struktur der Multiplett-S-Zustände in zweiatomigen Molekülen. I, *Z. Phys.*, 1929, **53**(5), 422–428, DOI: **10.1007/BF01347762**.

42 H. W. Bode, *Network Analysis and Feedback Amplifier Design*, D. Van Nostrand Company, incorporated 1945.

43 B. A. Boukamp, A Linear Kronig-Kramers Transform Test for Immittance Data Validation, *J. Electrochem. Soc.*, 1995, **142**(6), 1885, DOI: **10.1149/1.2044210**.

44 B. A. Boukamp, Electrochemical impedance spectroscopy in solid state ionics: recent advances, *Solid State Ionics*, 2004, **169**(1), 65–73, DOI: **10.1016/j.ssi.2003.07.002**.

45 J. E. B. Randles, Kinetics of rapid electrode reactions, *Discuss. Faraday Soc.*, 1947, **1**, 11–19, DOI: **10.1039/DF9470100011**.

46 A. C. Lazanas and M. I. Prodromidis, Electrochemical Impedance Spectroscopy–A Tutorial, *ACS Meas. Sci. Au*, 2023, **3**(3), 162–193, DOI: **10.1021/acsmeasuresciau.2c00070**.

47 L. Hu and X. Xu, Current Pulse-Based Measurement Technique for Zinc–Air Battery Parameters, *Energies*, 2023, **16**(18), 6448.

48 F. W. T. Goh, Z. Liu, T. S. A. Hor, J. Zhang, X. Ge, Y. Zong, A. Yu and W. Khoo, A Near-Neutral Chloride Electrolyte for Electrically Rechargeable Zinc-Air Batteries, *J. Electrochem. Soc.*, 2014, **161**, A2080, DOI: **10.1149/2.0311414jes**.

49 W. Kao-ian, R. Pornprasertsuk, P. Thamyongkit, T. Maiyalagan and S. Kheawhom, Rechargeable Zinc-Ion Battery Based on Choline Chloride-Urea Deep Eutectic Solvent, *J. Electrochem. Soc.*, 2019, **166**, A1063, DOI: **10.1149/2.0641906jes**.

50 M. Braig and R. Zeis, Distribution of relaxation times analysis of electrochemical hydrogen pump impedance spectra, *J. Power Sources*, 2023, **576**, 233203, DOI: **10.1016/j.jpowsour.2023.233203**.

51 M. Heinzmann, A. Weber and E. Ivers-Tiffée, Advanced impedance study of polymer electrolyte membrane single cells by means of distribution of relaxation times, *J. Power Sources*, 2018, **402**, 24–33, DOI: **10.1016/j.jpowsour.2018.09.004**.

52 J. Fu, J. Zhang, X. Song, H. Zarrin, X. Tian, J. Qiao, L. Rasen, K. Li and Z. Chen, A flexible solid-state electrolyte for wide-scale integration of rechargeable zinc–air batteries, *Energy Environ. Sci.*, 2016, **9**(2), 663–670, DOI: **10.1039/C5EE03404C**.

53 R. Franke-Lang and J. Kowal, Analysis of Electrochemical Impedance Spectroscopy on Zinc-Air Batteries Using the Distribution of Relaxation Times, *Batteries*, 2021, **7**(3), 56.

54 H. Ma and B. Wang, A bifunctional electrocatalyst α-MnO2-LaNiO3/carbon nanotube composite for rechargeable zinc–air batteries, *RSC Adv.*, 2014, **4**(86), 46084–46092, DOI: **10.1039/C4RA07401G**.

55 A. Kube, W. Strunz, N. Wagner and K. Andreas Friedrich, Evaluation of electrochemical impedance spectra of - batteries (Li-air/Zn-air) for aqueous electrolytes, *Electrochim. Acta*, 2021, **396**, 139261, DOI: **10.1016/j.electacta.2021.139261**.